

# Influence of cooling-induced compressibility on the structure of turbulent flows and gravitational collapse

Enrique Vázquez-Semadeni,

*Instituto de Astronomía, UNAM, Apdo. Postal 70-264, México, D. F. 04510, México*

*e-mail: enro@astroscu.unam.mx*

Thierry Passot and Annick Pouquet

*Observatoire de la Côte d'Azur, B.P. 229, 06304, Nice Cedex 4, France*

*e-mail: passot,pouquet@obs-nice.fr*

## ABSTRACT

We investigate the properties of highly compressible turbulence, the compressibility arising from a small effective polytropic exponent  $\gamma_e$  due to cooling. In the limit of small  $\gamma_e$ , the density jump at shocks is shown to be of the order of  $e^{M^2}$ , much larger than the  $M^2$  jump associated with high-Mach number flows in the isothermal regime. In the absence of self-gravity, the density structures arising in the moderately compressible case consist mostly of patches separated by shocks and behaving like waves, while in the highly compressible case clearly defined long-lived object-like clouds emerge. The transition from wave-like to object-like behavior requires a change in the relative phase of the density and velocity fields analogous to that in the development of an instability. When the forcing in the momentum equation is purely compressible, the rotational energy decays monotonically in time, indicating that the vortex-stretching term is not efficient in transferring energy to rotational modes. This property may be at the origin of the low amount of rotation found in interstellar clouds. Vorticity production is found to rely heavily on the presence of additional terms in the equations, such as the Coriolis force at large scales and the Lorentz force at small scales in the interstellar medium, or on the presence of local sources of heating. In the presence of self-gravity, we suggest that turbulence can produce bound structures for  $\gamma_e < 2(1 - 1/n)$ , where  $n$  is the typical dimensionality of the turbulent compressions. We support this result by means of numerical simulations in which, for sufficiently small  $\gamma_e$ , small-scale turbulent density fluctuations eventually collapse even though the medium is globally stable. This result is preserved in the presence of a magnetic field for supercritical mass-to-flux ratios. At larger polytropic exponents, turbulence alone is not capable of producing bound structures, and collapse can only occur when the medium is globally unstable. This mechanism is a plausible candidate for the differentiation between primordial and present-day stellar-cluster formation and for the low efficiency of star formation. Finally, we discuss models of the interstellar medium at the kpc scale including rotation, which restores a high- $\gamma_e$  behavior.

*Subject headings:* ISM: clouds – instabilities – magnetohydrodynamics – turbulence – Cosmology: miscellaneous

## 1. Introduction

Astrophysical flows are expected to be highly turbulent, with a wide variety of mostly compressible energy sources at various scales. Thus we can expect the nature of astrophysical turbulence to be quite different from standard laboratory turbulence, which is mainly a vortical phenomenon. If the flow is subject to strong heating processes and radiative cooling, with thermal time scales substantially shorter than the dynamical ones (Spitzer & Savedoff 1950), as is the case in the interstellar medium (ISM) or the post-recombination medium in cosmology, rapid thermal equilibrium can be established, and the fluid behaves as a polytropic gas in which  $P \propto \rho^{\gamma_e}$ , where  $\gamma_e$  is an equivalent polytropic exponent. Such systems have been discussed both in the linear (Elmegreen 1991) and nonlinear regimes (Vázquez-Semadeni et al. 1995, hereafter referred to as Paper I; Passot et al. 1995, hereafter Paper II). In particular, in the models of the ISM at the 10–1000 pc scales we have presented in previous work, the thermal time scales range from  $10^{-1}$  to  $10^{-4}$  times the dynamical timescales (Paper I; see also Elmegreen 1993a). For standard cooling functions (e.g., Dalgarno & McCray 1972), which depend on the metallicity and ionization fraction among other factors,  $\gamma_e$  can take values smaller than one and even negative (leading to the isobaric mode of the thermal instability). As  $\gamma_e$  approaches zero, pressure gradients are almost absent, leading to a rather inelastic behavior with a very high compressibility, a behavior which is reminiscent of Burgers flows even when the Mach number based on the isothermal sound speed (the quantity normally reported in observational studies) is of order unity.

In this paper we investigate the influence of the degree of compressibility of the flow (measured by either the effective polytropic index  $\gamma_e$  or the actual Mach number  $M_a$ ) on both the properties of the turbulence and the mechanisms of formation of density structures. It is important to predict whether turbulence is dominated by vortical or compressible motions, depending on the type of forcing imposed on the flow, and the additional physical processes considered. In particular, it is of interest to investigate the nature of the transfer between compressible and rotational modes of the velocity field. This problem has been investigated in the low-to-moderate compressibility regimes by Kida & Orszag (1990a,b), who found that transfer occurs mostly from rota-

tional to compressible modes, and only in an efficient manner above  $M_a \sim 0.3$  (see also Passot & Pouquet 1987). In the present paper we extend their results to the highly compressible regime, and use two- and three-dimensional numerical simulations to show that, for purely compressible forcing (such as that originating from stellar winds), vorticity decreases steadily. We also discuss alternative vorticity production mechanisms, such as the baroclinic term or the presence of shear, the Coriolis force, and magnetic fields. Throughout the paper, we address the discussion mostly towards processes in the interstellar medium at various scales, although we consider generalizations which should be applicable to a wider variety of astrophysical flows, in particular in Cosmology and in molecular clouds.

In the context of the ISM, both the amplitude and persistence of density fluctuations are highly dependent on the degree of compressibility of the flow, and thus the latter can affect the cloud and star formation mechanisms. In the linear regime, Elmegreen (1989) has proposed that the gravitationally unstable scales are greatly reduced in the presence of dissipation through cloud collisions, while Renard & Chièze (1993) have studied the modifications to the Jeans length in the vicinity of the thermal instability. In addition, various workers have discussed the formation of self-gravitating clouds induced by external velocity fields (e.g., Hunter & Fleck 1982; Hunter et al. 1986; Elmegreen 1993a; Paper I; Padoan 1995), although without consideration of the direct dependence on an effective polytropic index  $\gamma_e$ . In this paper we also discuss, based on numerical simulations, the ability of turbulence to form gravitationally bound structures which are the sites of star formation, as well as their characteristic scales, in relation to  $\gamma_e$ . This problem will be addressed in the context of both a polytropic gas (either with a single value of  $\gamma_e$  or a piecewise index depending on the density) and a fully thermodynamic model of the ISM including parameterized heating and cooling, as introduced in Paper I and, with rotation and magnetic field (Paper II). Note that in this paper we only consider the large-scale effects of turbulence in the formation of density structures, neglecting its well known effects for cloud support at small scales (e.g., Chandrasekhar 1951; Bonazzola et al. 1987; Léorat et al. 1990; Vázquez-Semadeni & Gazol 1995; see also the review by Scalo 1987 and references therein). However, our results should also be applicable to a cloud-

fluid in which the pressure includes a sub-grid turbulent component (e.g., Hunter & Fleck 1982; Scalo & Struck-Marcell 1984; Elmegreen 1991); sub-grid cloud collisions provide an effective power-law “cooling” mechanism (e.g., Elmegreen 1991).

The outline of the paper is as follows. In the next section we describe the numerical approach and define the various models. Section 3 is devoted to the influence of various degrees of compressibility on randomly forced compressible turbulence, when the forcing is only in the velocity equation and is only potential, and to the production of vorticity in the highly compressible regime by the vortex-stretching term and other mechanisms, in two and three dimensions. The next Section then deals with the implications for scale-free astrophysical flows when self-gravity and magnetic fields are included. Section 5 considers the results of the previous sections in the context of models of the ISM at the kpc scale based on the one presented in Paper II. Finally, § 6 is the conclusion.

## 2. The models

In this paper we use several sets of hydrodynamic equations to simulate highly compressible flows, ranging from a simple barotropic flow to the full model of the ISM used in Paper II (with the addition of winds or a random forcing  $\mathbf{F}_c$  in the velocity equation). The latter reduces to the following equations, which represent the ISM on the plane of the galactic disk:

$$\frac{\partial \rho}{\partial t} + \nabla \cdot (\rho \mathbf{u}) = \mu \nabla^2 \rho, \quad (1)$$

$$\begin{aligned} \frac{\partial \mathbf{u}}{\partial t} + \mathbf{u} \cdot \nabla \mathbf{u} = & -\frac{\nabla P}{\rho} - \left(\frac{J}{M_a}\right)^2 \nabla \phi + \\ & \frac{1}{\rho} (\nabla \times \mathbf{B}) \times \mathbf{B} - 2\Omega \times \mathbf{u} - \nu_8 \nabla^8 \mathbf{u} + \\ & \nu_2 (\nabla^2 \mathbf{u} + \frac{1}{3} \nabla \nabla \cdot \mathbf{u}) + \mathbf{F}_s + \mathbf{F}_c, \end{aligned} \quad (2)$$

$$\begin{aligned} \frac{\partial e}{\partial t} + \mathbf{u} \cdot \nabla e = & -(\gamma - 1)e \nabla \cdot \mathbf{u} + \kappa_T \frac{\nabla^2 e}{\rho} + \\ & \Gamma_d + \Gamma_s - \rho \Lambda, \end{aligned} \quad (3)$$

$$\frac{\partial \mathbf{B}}{\partial t} = \nabla \times (\mathbf{u} \times \mathbf{B}) - \nu_8 \nabla^8 \mathbf{B} + \eta \nabla^2 \mathbf{B}, \quad (4)$$

$$\nabla^2 \phi = \rho - 1, \quad (5)$$

$$P = (\gamma - 1)\rho e, \quad (6)$$

$$\Gamma_d(\mathbf{x}, t) = \Gamma_o(\rho/\rho_{ic})^{-\alpha}, \quad (7)$$

$$\Gamma_s(\mathbf{x}, t) = \begin{cases} \text{constant} & \text{if } \rho(\mathbf{x}, t_0) > \rho_{cr} \\ & \text{and } 0 < t - t_0 < \Delta t_s, \\ 0 & \text{otherwise} \end{cases}, \quad (8)$$

and

$$\Lambda = \Lambda_i T^{\beta_i} \quad \text{for } T_i \leq T < T_{i+1}, \quad (9)$$

where

$$\begin{array}{lll} T_1 = 100 & \Lambda_1 = 1.14 \times 10^{15} & \beta_1 = 2 \\ T_2 = 2000 & \Lambda_2 = 5.08 \times 10^{16} & \beta_2 = 1.5 \\ T_3 = 8000 & \Lambda_3 = 2.35 \times 10^{11} & \beta_3 = 2.867 \\ T_4 = 10^5 & \Lambda_4 = 9.03 \times 10^{28} & \beta_4 = -0.65 \\ T_5 = 4 \times 10^7. \end{array}$$

The temperature  $T$  is measured in  $K$  and  $\Lambda$  in  $\text{erg s}^{-1} \text{g}^{-2} \text{cm}^3$ . Note that the stellar heating  $\Gamma_s$  is spread out on a few pixels around a stellar center by a convolution with a Gaussian profile. In eq. (8),  $t_0$  is the time at which the density threshold  $\rho_{cr}$  is reached at point  $\mathbf{x}$  (see Paper I and II for further details).

As usual,  $\rho$  is the density,  $\mathbf{u}$  is the fluid velocity,  $e$  is the internal energy per unit mass,  $P$  is the thermal pressure,  $\mathbf{B}$  is the magnetic induction,  $\Omega$  is the angular velocity of the rotation, and  $\phi$  is the gravitational potential. The ratio  $\gamma = c_p/c_v$  of specific heats at constant pressure and volume respectively is  $\gamma = 5/3$ . The temperature is related to the internal energy by  $e = c_v T$ . The nondimensionalization is the same as in Paper II; the resulting nondimensional parameters are  $J$ , the number of Jeans lengths in the integration box, whose side is  $2\pi$ , and  $M_a$ , the Mach number corresponding to the characteristic velocity  $u_0$  at the initial mean temperature of the flow (note that we take  $c_v = [\gamma(\gamma - 1)M_a^2]^{-1}$ ). The magnetic field is written as  $\mathbf{B} = B_0 \mathbf{e}_x + \mathbf{b}$  where  $B_0$  represents the uniform azimuthal component of the field, and  $\mathbf{b}$  a superimposed fluctuating component. The shearing forcing  $\mathbf{F}_s$  is accomplished by fixing one component of the largest Fourier mode in order to impose a velocity profile  $u_x = -0.375 \sin y$ ; the additional term  $\mathbf{F}_c$  is discussed further below.

These equations are solved both in two and three dimensions with periodic boundary conditions, using a Fourier pseudospectral technique with a resolution of  $128^2$  collocation points for two-dimensional runs and  $64^3$  for the three-dimensional ones. A hyperviscosity scheme with a  $\nabla^8$  operator is used, which confines viscous effects to the smallest resolved scales and allows for the use of much smaller values of the

kinematic viscosity  $\nu_2$  and magnetic diffusivity  $\eta$  than what would be possible when  $\nu_8 = 0$ . The adjunction of the second-order viscosity and diffusivity, compared to the model used in Paper I and Paper II, has been made necessary in the highly compressible regime in order to “filter” out the oscillations in the vicinity of strong shocks (Passot & Pouquet 1988). In addition, a mass diffusion  $\mu \nabla^2 \rho$  is added to the continuity equation in order to smooth out the density gradients, thus allowing the simulations to reach higher r.m.s. Mach numbers. The values of the various coefficients for the 128<sup>2</sup> runs are  $\nu_8 = 8 \times 10^{-12}$ ,  $\nu_2 = \eta = 2 \times 10^{-3}$ ,  $\mu = 3 \times 10^{-2}$  and  $M_a = 1$  throughout the paper. For the 3D runs we take  $\nu_8 = 10^{-9}$ ,  $\nu_2 = 2.5 \times 10^{-3}$ , and  $\mu = 4 \times 10^{-2}$ . We refer the reader to Paper II for further details concerning the technique and the model terms. The additional acceleration  $\mathbf{F}_c$  introduced in the velocity equation has been taken either as a random vector field with a  $k^{-4}$  power-law spectrum peaked at a wavenumber  $k_{\text{for}}$ , white noise in time and with an adjustable ratio  $r_c$  of compressible to solenoidal components, or as a wind-mimicking momentum source of the form  $\mathbf{F}_c = -\nabla \psi$ , where  $\psi$  is proportional to the stellar heating  $\Gamma_s$ . Finally, the initial conditions for all variables are Gaussian fluctuations with random phases. For the velocity field, the fraction of solenoidal to compressible energy is an additional adjustable parameter.

According to the results of Paper I and Paper II, due to the short thermal time scales, the flow behaves essentially as a piecewise polytropic gas, except in the regions of star formation. As a consequence, we also solve a simplified set of equations (hereafter denoted *ppm*, for Piecewise Polytropic Model) in which we eliminate the internal energy equation and use a piecewise polytropic equation of state given by

$$P = a\rho^{\gamma_{e_i}} \equiv \left[ \frac{\Gamma_o \rho_{\text{ic}}^\alpha}{\Lambda_i} \right]^{1/\beta_i} \frac{\rho^{\gamma_{e_i}}}{\gamma M_a^2}, \quad (10)$$

with  $i = 1, \dots, 5$ , in conjunction with the five temperature domains of eq. (9). Note that in the barotropic case the nondimensionalization of the equations leads to an explicit factor of  $M_a^{-2}$  in the pressure, the sound speed in the equilibrium state of temperature  $T_{\text{eq}}$  being given by  $c_e^2 = (\gamma_e/\gamma M_a^2) T_{\text{eq}}$ . The effective polytropic index is given, in terms of the exponents  $\beta_i$  in (9) and  $\alpha$  in eq. (7), by:

$$\gamma_{e_i} = 1 - (1 + \alpha)/\beta_i. \quad (11)$$

Note that  $\gamma_{e_i}$  was noted  $\gamma_{eff}$  in Paper II, but the

present notation stresses its dependence on the interval of temperature in the cooling function. Finally, the boundaries of the different temperature ranges in the cooling function for the full model correspond to densities given by

$$\rho_i = \left( \frac{\Gamma_o \rho_{\text{ic}}^\alpha}{\Lambda_i} \right)^{\frac{1}{1+\alpha}} T_{i+1}^{-\frac{\beta_i}{1+\alpha}}. \quad (12)$$

For convenience, we adjust the degree of compressibility of the flow (the value of  $\gamma_{e_i}$ ) by varying the exponent  $\alpha$  of the diffuse heating. This is equivalent to varying the exponents  $\beta_i$  in all intervals of the cooling function. Although this is not a very realistic approach, it provides us with the simplest means for varying the flow’s “hardness”, i.e. the flow’s resistance to compression. Actual modifications to the cooling function will be discussed in a future paper (Franco et al. 1996).

A further level of simplification, useful to single out purely fluid dynamical properties of supersonic turbulence, consists of using a single polytropic exponent  $\gamma_e$ . In this case, the pressure is taken as  $P = (\gamma_e M_a^2)^{-1} \rho^{\gamma_e}$ , leading to a sound speed  $c_e = (1/M_a)$  in the equilibrium state  $\rho = 1$ . In the following, we refer to these equations as the B-model, for Barotropic model.

Throughout the paper, we will refer to a rather large number of simulations, whose most relevant parameters are summarized in Table 1.

### 3. Some properties of highly compressible flows

#### 3.1. Density structures

As discussed in the introduction, low values of  $\gamma_e$  lead to very high compressibilities, and in fact the degree of compression reached in this case is much higher than the one obtained by increasing the Mach number. This can be seen by calculating the density jump  $X \equiv \rho_2/\rho_1$  across a shock in a barotropic gas of index  $\gamma_e$ . It is easy to show that  $X$  satisfies

$$X^{1+\gamma_e} - (1 + \gamma_e M^2)X + \gamma_e M^2 = 0, \quad (13)$$

where  $M$  is the Mach number upstream of the shock. From this equation, we recover the fact that the compression ratio for an isothermal shock ( $\gamma_e = 1$ ) is  $M^2$ , but we also see that, for  $\gamma_e \ll 1$ ,  $X$  is approximately given by  $X \sim (1 + \gamma_e M^2)^{1/\gamma_e}$ . For a fixed value of  $M$ , this expression tends to  $e^{M^2}$  as  $\gamma_e \rightarrow 0$ , a density

jump which can be much larger than the isothermal one.

We now discuss the nature of the density condensations present in the flow as observed in our simulations, and their relation to the value of the polytropic exponent. For simplicity, we consider the B-model and the *ppm* equations, with a purely compressible random forcing in the velocity equation.

Even though the boundary between moderate and high compressibility is not sharp, the two regimes lead to quite different density structures. In the former case, the density field consists of patches separated by shocks, and whose lifetime is the sound crossing time within the patches. This is illustrated in fig. 1 (left), where we display a typical snapshot of the density field in a simulation labeled run 63, with  $\gamma_e = 1.5$  and  $k_{\text{for}} = 4$ . Note that the highest peaks form at the intersection of shocks. Such a behavior is analogous to what is observed in decaying flows, both in 2D (Passot et al. 1988) and in 3D (Porter et al. 1994).

As  $\gamma_e$  is lowered, the density peaks become higher and narrower, and have longer lifetimes since the effective sound speed decreases. This is illustrated in fig. 1 (right), showing the density field of run 65, with  $\gamma_e = 0.3$ . In fact, when using the *ppm* equations with the fiducial values of the parameters used in Paper II ( $\alpha = 0.5$ ),  $\gamma_e$  can locally reach zero for intermediate densities, and we then observe a transition of behavior from wave-like to object-like. We exemplify this behavior in fig. 2, which shows the density field of two two-dimensional simulations using the *ppm* equations, the first one with  $\alpha = -0.5$  (run 54, left), and the second with  $\alpha = 0.5$  (run 53, right).

In order to understand the distinction between wave-like and object-like behavior, consider a passive scalar, which is defined as a quantity  $s$  obeying the pure advection equation  $\partial s / \partial t = -\mathbf{u} \cdot \nabla s$ , and consider its motion relative to a density perturbation. We define an object as a density perturbation within which the passive scalar remains for a substantial period of time, whereas in a wave the passive scalar and the density fluctuations drift apart. For example, a one-dimensional wave packet  $\rho = \rho(x - u_0 t)$ , moves as a whole at speed  $u_0$ . Adams et al. (1994) have shown that, in the context of a logatropic equation of state of the form  $P \sim c_e^2 \rho + p_0 \log(\rho / \rho_R)$  such wave packets can behave as solitary waves. Conservation of mass leads to  $(u - u_0)\rho = cst$ , showing that the fluctuations of  $\rho$  and  $u$  are “in phase” (fig. 3; see also fig. 2 of Paper II). The scalar  $s$ , advected at the flow veloc-

ity  $u \neq u_0$ , will as a consequence drift with respect to the density perturbation. On the other hand, in the case of an object (i.e., a density clump), the velocity field is either convergent towards its center (“out of phase” with the density perturbation), or is zero inside and contains two accretion shocks at its edges so that the passive scalar remains within the boundaries of the density fluctuation. The transition from wave to object can spontaneously happen when the flow becomes unstable, e.g. thermally or gravitationally. In the presence of turbulence this behavior is continuously approximated as the polytropic exponent approaches zero. In this case, the flow behaves almost as a Burgers flow, with large density peaks at shock locations instead of the density jumps appearing in flows with finite pressure. Therefore, the clouds have long lifetimes and are only affected by collisions with other clouds. Note that in the limiting case of zero pressure gradient, cloud (shock) collisions become entirely coalescing (“sticky”), since disruption requires the presence of vorticity, whose dynamics is discussed in the next section.

### 3.2. Evolution of vorticity in highly compressible turbulence

#### 3.2.1. The role of vortex stretching

It is first useful to write the equations for the potential vorticity  $\omega_p \equiv \omega / \rho = (\nabla \times \mathbf{u}) / \rho$  and the dilatation  $\nabla \cdot \mathbf{u}$  in the barotropic case. Neglecting the dissipation terms proportional to  $\nu_8$  and  $\nu_2$ , they read

$$\frac{\partial \omega_p}{\partial t} + \mathbf{u} \cdot \nabla \omega_p = \omega_p \cdot \nabla \mathbf{u} \quad (14)$$

$$\frac{\partial \nabla \cdot \mathbf{u}}{\partial t} + \nabla^2 \frac{u^2}{2} - \omega^2 + \mathbf{u} \cdot \nabla \times \omega + \frac{a\gamma_e}{\gamma_e - 1} \nabla^2 \rho^{\gamma_e - 1} = \nabla \cdot \mathbf{F}_c. \quad (15)$$

Note that these equations are asymmetrical: dilatation can easily be produced out of rotational motions (from the  $-\omega^2$  term), whereas vorticity production can only originate from the vortex-stretching term  $\omega_p \cdot \nabla \mathbf{u}$  in three dimensions (3D) (see also Kornreich & Scalo 1996). In the two-dimensional inviscid case, it is well known that there is conservation of any functional of the potential vorticity (e.g., Pedlovsky 1987) in the absence of shocks. When oblique shocks are present, the vorticity contained in them will be dissipated much more rapidly than elsewhere in the flow in the presence of viscosity. Moreover, since  $\omega_p$  obeys a passive scalar equation (in 2D), the vorticity

$\omega$  (which is larger in dense regions) will tend to be confined inside clouds or at their edges in the highly compressible regime, in which, as mentioned in §3.1, clouds behave as objects. This was observed in the simulations of the full model with  $\alpha = 0.5$  (Paper II), but not in those of Paper I with  $\alpha = 0$ , *i.e.* with a higher  $\gamma_e$ .

We now examine whether the vortex-stretching term can contribute significantly to the transfer of energy from the compressible to the solenoidal modes of the velocity. Note that, even though in 3D the presence of the vortex stretching term does not allow us to draw any conclusion regarding the conservation of  $\omega_p$ , it is nevertheless relevant to consider the equation for this quantity, since it avoids the need to take into account the compression term  $-\omega \nabla \cdot \mathbf{u}$  in the vorticity equation, which only reflects mass conservation.

Kida & Orszag (1990a) have investigated the transfer between internal modes and compressible and rotational kinetic modes in three dimensional, forced, compressible turbulence at moderate Mach numbers. They find a negligible transfer between the compressible and rotational kinetic modes. Here we extend this analysis to highly compressible flows, using the *ppm* equations. Starting with 100% solenoidal motions, and stirring the flow with a purely potential acceleration, we observe, for a wide range of values of  $\gamma_e$ , that the ratio of rotational to total kinetic energy per unit mass <sup>1</sup>  $e_s/e_k$  always decays, as shown in fig. 4. Together with other runs discussed below in §3.3.1, this figure shows the evolution of  $e_s/e_k$  for two 3D runs at resolution  $64^3$  solving the *ppm* equations, one with  $\alpha = 0.5$  (run 60), and the other with  $\alpha = -0.5$  (run 67). The latter is thus “harder”. Note also that, after the initial transients have subsided, the rate of decay appears to be independent of  $\gamma_e$ , at least for the range of values considered here. Thus, the stretching term does not appear to contribute to energy transfer from the compressible to the rotational modes.

The above result is rather unexpected, since vortex stretching is the main mechanism for vorticity production in incompressible turbulence. Instead, for highly compressible flows, vortex stretching appears to contribute mostly to the destruction of potential vorticity. We suggest the following mechanism. Let us first consider the case in which potential vorticity is a small perturbation on an irrotational flow. Since

eq. (14) is identical to that for the magnetic field, it is legitimate, in analogy with the kinematic dynamo mechanism, to investigate whether  $\omega_p$  can increase on scales large compared to that of the potential flow, assumed given. As is well known (e.g., Krause & Rädler 1980), the growth of the magnetic field in a slow dynamo happens through the presence of helicity in the flow. In the present case, however, the helicity of the basic flow is identically zero, rendering the growth of potential vorticity unlikely at dominant order. Nevertheless, we must consider the possible amplification of  $\omega_p$  on a scale comparable to that of the basic flow (as in the context of the fast dynamo problem). In order to investigate this problem, a knowledge of the structure of the basic flow is necessary. As discussed in the previous section (see fig. 1), the highly compressible regime is dominated by the presence of locally two-dimensional sawtooth shocks (see also Kadomtsev & Petviashvili 1973). As already observed by Kida & Orszag (1990b), vortex lines tend to be antiparallel with density (and velocity) gradients. A possible explanation of this observation is that, on both sides of a shock, the velocity gradient matrix has positive eigenvalues, which tend to amplify vortex fluctuations in the direction perpendicular to the shock, while the vortex stretching term would have no effect on vortex lines orthogonal to the density gradient. However, while the vorticity is amplified in these expansion regions, it is also advected towards the shock from both sides, where it is then destroyed since the velocity gradient matrix has negative eigenvalues in these regions of strong compression. In summary, in highly compressible regimes, shocks are expected to act like sinks in which potential vorticity is drained from the flow.

In the fully nonlinear case where rotational modes are initially of the same order of magnitude as compressive ones, the numerical experiments shown in fig. 4 indicate that the decay of rotational energy persists, suggesting that the above mechanism is still at play.

### 3.2.2. The baroclinic term

Another important source of vorticity in the fully thermodynamic case is the so-called baroclinic term,  $\nabla P \times \nabla \rho / \rho^2$ , which is known to be active behind curved shocks or at their collisions (Passot & Pouquet 1987; Fleck 1991; Klein & McKee 1994). To test its effect, we have performed a new simulation, run 68, identical to run 60 described above, but using the full thermodynamic equations. We find that

<sup>1</sup>Note that the integrated energies per unit volume and per unit mass typically differ by no more than a few percent.

the rotational modes still decrease steadily in time, as also shown in fig. 4. This indicates that the baroclinic term has a globally negligible contribution to the vorticity production, being overwhelmed by the draining effect of the vortex-stretching term in negative dilatation regions. This remark is corroborated by the observation made by Porter et al. (1995) that on average the baroclinic term is  $\sim 20$  times smaller than the stretching term in compressible flows forced by an external shear. Note that, behind the intersection of shocks, vorticity creation can be locally important (Passot & Pouquet 1987), whereas in other regions the pressure and density gradients are always close to parallel (Kida & Orszag 1990b).

In fact, vorticity production behind shocks does not require the contribution of the baroclinic term (Hayes 1957), the production mechanism relying on simple geometrical considerations. In the present simulations such vorticity production is not seen, possibly due to the lack of resolution or to the fact that the shocks that form remain straight (occurrence of such vorticity production has been observed in high-resolution simulations of collisions of strong SN shock waves with spherical molecular clouds (Klein & McKee 1994)). The presence of the baroclinic term does not change this conclusion and is only important, as we shall see, when thermal heating is present (§ 3.3.3).

### 3.3. Other mechanisms of vorticity production

Since the nonlinear and baroclinic terms have been found in the previous sections to be globally insufficient for vorticity production and maintenance in the presence of high compressibility and purely compressible forcing, it is important to examine alternative sources of vorticity in astrophysical flows. As an example, we will consider the case of the ISM at the kpc scale, within which possible agents for vorticity production are the Galactic disk rotation, various heat sources and the magnetic field.

#### 3.3.1. Coriolis force

It is well known that the Coriolis force can convert converging motions into shearing ones. In fig. 4 we also show the time evolution of the ratio  $e_s/e_k$  for the three dimensional run labeled run 69, analogous to run 60, but with the addition of the Coriolis force with  $\Omega = 0.4$  in code units, corresponding to the fiducial value  $2\pi/2 \times 10^8 \text{ yr}^{-1}$  (see Paper II). It is notice-

able that compressible and rotational modes almost reach equipartition after  $4 \times 10^7 \text{ yr}$ . Compared to the run without the Coriolis force (run 60), with the same random forcing, run 69 develops 30% less density fluctuations but twice as much kinetic energy, while the internal energy remains approximately at the same level. The increase of the level of kinetic energy is probably due to the fact that compressible motions dissipate faster than rotational ones and thus, for a given energy input rate, the equilibrium kinetic energy will be larger if rotational modes are excited. Additionally, it is interesting to estimate the importance of the Coriolis force at different scales. For economy we do this in two-dimensions. The Rossby number (measuring the relative size of the Coriolis force with respect to the nonlinear advection term), scales as  $L^{1/2}$  if we assume that the velocity dispersion  $u$  scales roughly as  $L^{1/2}$  (Larson 1981; Falgarone et al. 1992). A run using  $\Omega = 0.05$  (run 85), a value appropriate for scales  $\sim 25 \text{ pc}$ , ends up with only  $\sim 5\%$  of rotational energy, while a run with  $\Omega = 0.4$  (run 57, appropriate for the kpc scale) typically contains  $\sim 50\%$  of rotational energy. Interestingly, this value is very similar to the 3D case, run 69. This indicates that the Galactic Coriolis force is likely to be an important source of vortical motions at the kpc scale, but not at the molecular cloud scale.

#### 3.3.2. Large-scale shear from differential rotation

Another agent due to the Galactic rotation is the shear arising from its differential character. A run with an imposed shear as performed in Paper II corresponding roughly to Oort's A constant (run 59), shows a selective creation of vorticity of the same sign as that of the imposed shear. For this run,  $e_s/e_k \sim 30\%$  on average.

#### 3.3.3. Local heating

The stellar heating  $\Gamma_s$  provides another source of vorticity in the flow. Indeed, at locations where thermal energy is injected, the baroclinic term will be important, since the gradients of density and temperature cease to be correlated. This effect is most noticeable in the dynamics of expanding shells, which propagate without deformation when only wind-type forcing is included in the equations, while they distort and fragment in the presence of stellar heating. This is illustrated in fig. 5, which shows the density fields for runs 28 (left) and 35 (right). These runs start with purely compressible velocity fluctuations

and differ only in that the forcing in run 35 is in the velocity (through  $\nabla\psi$ ; cf. § 2), while run 28 has thermal energy forcing only (through  $\Gamma_s$ ). The production of solenoidal energy is substantial in run 28 in which, during the period of shell breakup,  $e_s/e_k \sim 0.5$ , while in run 35,  $e_s/e_k$  barely reaches 0.01. Note that the low value of  $e_s/e_k$  in run 35 is in agreement with the result of §3.2.2 that the production of vorticity behind curved shocks is negligible in the absence of external heating.

Note that the breakup of shells in the presence of heating can also be interpreted as a consequence of linear Vishniac-type instabilities, occurring in fronts between thermal and ram pressures (Vishniac 1983). However, the present simulations do not allow us to decide whether the shells break due to vorticity production by the baroclinic term, to the linear Vishniac instability, or both. This is because in these runs actually a thin shell of star-forming sites forms immediately behind the gas shell, causing the baroclinic term to be large there. One indication is that in run 35, with wind-type forcing, the nonlinear Vishniac instability (Vishniac 1994; see also Hunter et al. 1986; Stevens, Blondin & Pollack 1992) does not develop, suggesting that the present simulations lack the necessary resolution. A detailed examination of this problem would require monitoring of the baroclinic term and possibly higher-resolution simulations. This, however, is beyond the scope of the present paper. Here we just record the importance of local heating as a source of vorticity.

### 3.3.4. Magnetic field

Finally, we discuss the effect of the Lorentz force on the transformation of compressive motions into rotational ones. For this purpose, we have performed four runs with the *ppm* model labeled runs 86, 84, 87 and 88, identical to run 53 except for the inclusion of a uniform initial magnetic field along the  $x$ -axis, with strengths of, respectively, 0.05, 0.3, 1, and 3, in nondimensional code units (at  $B_o = 1$ , the Alfvén velocity  $v_a = u_0$ , see Paper II). A small fluctuating field with an rms amplitude of 0.01 is also included. In fig. 6 we show the time evolution of the fraction of specific kinetic energy in solenoidal motions  $e_s/e_k$  for the four runs. The fraction of energy in solenoidal modes is seen to increase with  $B_o$  until equipartition with compressible modes is reached at values of  $B_o > 1$ . The fluctuating magnetic energy obeys the same trend (fig. 7), as already mentioned in Paper II

in the context of the full model. In fig. 7, temporal oscillations are observed, whose frequency is roughly proportional to  $B_o$ . However, these oscillations do not appear to be due only to Alfvén waves. Instead, fully developed MHD turbulence is present, as can be inferred from the presence of locally strong currents – indicating small-scale intermittent magnetic structures – and a power-law magnetic spectrum (fig. 8). The increase of the solenoidal energy in the form of fully developed turbulence with the uniform component of the magnetic field is remarkable and might, at first sight, appear contradictory to common assumptions (Elmegreen 1993b, sect. VII; Mouschovias 1991). This phenomenon of creation of vorticity by magnetic fields is important as well in the context of accretion disks (Vishniac & Diamond 1992).

The relative importance of the Lorentz force in the momentum equation increases as smaller scales are considered. For instance, taking typical values of the fluctuating magnetic field strength of  $\sim 5\mu\text{G}$  at the kpc scale and  $\sim 30\mu\text{G}$  at scales  $\sim 5$  pc, and typical velocity dispersions of respectively 10 and 2 km s $^{-1}$ , the ratio of the Lorentz force to the nonlinear advection term is roughly 20 times larger at the 5 pc scale. Thus, the production of vorticity from compressive motions due to the Lorentz force is most efficient at molecular cloud scales.

## 4. Scale-free flows with self-gravity

### 4.1. Influence of $\gamma_e$ on the formation of collapsing structures

The results presented in the previous sections have implications for star formation, since the ability of turbulence to form self-gravitating clouds depends on the compressibility of the flow. A simple estimate for the required values of  $\gamma_e$  for this to occur can be given as follows. Consider a medium with an effective polytropic exponent  $\gamma_e$ , for which the effective Jeans length is given by

$$L_{\text{eff}} = \left[ \frac{\gamma_e \pi c_i^2}{G \rho_0^{2-\gamma_e}} \right]^{1/2} = \sqrt{\frac{\gamma_e}{\gamma}} \rho_0^{\frac{\gamma_e-1}{2}} L_J, \quad (16)$$

where  $c_i$  is the isothermal sound speed such that  $P = c_i^2 \rho$  and  $L_J$  is the Jeans length based on  $c_i$ . The critical density at which the scale  $L$  becomes unstable is then given by  $\rho_J \propto L^{2/(\gamma_e-2)}$ . In order to account for turbulent compressions acting on  $n$  directions, we consider a volume  $V = L^n L_0^{3-n}$ , where  $L$  is the side of the volume which varies upon compression, and  $L_0$

is the side that remains unaltered. The critical mass to destabilize this volume is thus given by

$$M_J \propto L^{n+\frac{2}{\gamma_e-2}} L_0^{3-n}. \quad (17)$$

If  $M_J$  is a decreasing function of  $L$ , turbulent compression can produce gravitationally unstable structures, similarly to Hoyle’s (1953) notion of hierarchical gravitational fragmentation. Setting the exponent of  $L$  to zero then gives the critical value of the polytropic exponent as a function of the dimensionality of the compression  $n$ . In particular,

$$\gamma_c = \begin{cases} \frac{4}{3} & \text{for } n = 3 \\ 1 & \text{for } n = 2 \\ 0 & \text{for } n = 1. \end{cases} \quad (18)$$

This result thus recovers the well-known critical values of  $\gamma_e$  for the existence of equilibrium solutions of self-gravitating polytropic gas configurations (e.g., Chandrasekhar 1961), although within the different context of  $n$ -dimensional turbulent compressions. In the present case, this criterion describes the threshold value  $\gamma_c$  of  $\gamma_e$  at which the internal energy of a turbulent fluctuation increases more slowly upon compression than its gravitational energy. Conversely, above  $\gamma_c$ , a fluctuation can never be rendered unstable upon compression. Note that for  $\gamma_e < 0$ , no compression is necessary because the medium is then thermally unstable.

If we extend this result to non-integer values of  $n$ , accounting for clouds with fractal boundaries of typical dimension 1.4 (Falgarone et al. 1991), and recalling that the compression is likely to be driven by quasi-planar shocks (see also Fleck 1996), we obtain that  $0 < \gamma_c \leq 1$ , which is probably not unrealistic.

In order to examine the interplay between turbulence, compressibility and self-gravity, we have performed a series of forced runs with the B-model, using barotropic exponents of 0.9, 0.3 and 0.1 (runs 106, 107 and 108 respectively) and the same Jeans length  $L_{\text{eff}} = 2\pi/J$  (which is independent of  $\gamma_e$ , a fact following from the form of the pressure for the B-model), with  $J = 0.9$ . Note that all these runs are stable according to the linear criterion. The evolution of the maximum density within the integration box for runs 106, 107, and 108 is shown in fig. 9. The turbulent density fluctuations never grow in the case of the high-gamma run, but in the case of runs 107 and 108, local fluctuations eventually collapse, slightly earlier in the latter run, confirming earlier speculations by

various workers (e.g., Hunter & Fleck 1982; Bonazzola et al. 1987; Léorat et al. 1990; Padoan 1995) and extending the results of Hunter et al. (1986) for isolated gas streams to the fully turbulent regime. In fact, given the identical initial conditions and random forcing used in the two runs, the condensation that collapses in run 108 also forms in run 107, but is unable to actually collapse.

It is important to emphasize that the collapse in the turbulence-induced fluctuations is at small scale, contrary to the type of collapse expected for the linearly unstable case. To show this, we have performed an additional forced run with  $J = 1.1$  and  $\gamma_e = 0.9$  (run 109). Contours of the logarithm of the density field for runs 109 and 108 are presented in fig. 10, in which the left frame corresponds to run 109 and the right frame to run 108. The large void around the condensation in run 109 shows that most of the mass in the simulation is involved in the collapse, while significant amounts of matter are present outside the condensation for run 108. Also, note that the “stable” run (run 108) takes a rather long time ( $t = 14$ ) to finally develop a collapsing cloud, since a strong enough turbulent fluctuation is required, which is statistically unlikely. This may be an appropriate mechanism behind the low efficiency of star formation observed in the ISM (see, e.g., Evans 1991). Instead, run 109, which is globally unstable, collapses at  $t = 8.6$ , a time consistent, within a factor of 1.5, with the free-fall time  $t_{\text{ff}} \equiv L_J/c = 2\pi/(J\rho) = 5.7$  in code units.

Finally, we note that the runs described in this section, although providing strong support for the validity of the criterion (17), cannot be used to determine the actual value of  $\gamma_c$ , since in order to do this it would be necessary to verify that arbitrarily large density fluctuations do not collapse, which for large  $\gamma_e$  would require very large Mach numbers. Moreover, the dimensionality  $n$  of individual shocks may vary, and therefore the value of  $\gamma_c$  is probably meaningful only in a statistical sense.

#### 4.2. Magnetic field and self-gravity

We now investigate whether this mechanism is also at play in the presence of a uniform magnetic field  $B_0$ , which we take along the  $x$ -direction. The instability criterion of the uniform-density state is unchanged compared to the non-magnetic case (which reads  $J > 1$ ), except for perturbations exactly perpendicular to the field, for which the corresponding condition reads  $J^2 > 1 + B_0^2$  (Chandrasekhar 1961).

Again, note the independence on  $\gamma_e$  in these criteria in the context of the B-model. We have performed a forced run similar to run 109 but with  $B_o = 2$  in code units (run 111). This run, with  $J = 1.1$  and  $\gamma_e = 0.9$ , undergoes contraction along the field lines, but the resulting slab remains stable in the direction transverse to the field. Note that the critical value  $B_1$  of the uniform magnetic field for linear stability of the slab should be in fact larger than that corresponding to the transverse stability of the uniform state. A similar run with  $\gamma_e = 0.3$  (run 114) also forms a slab, but the turbulence is able to create a subcondensation within the slab which collapses gravitationally, thus exhibiting the same qualitative behavior as that reported in the previous subsection for the non-magnetic case. This is illustrated in fig. 11, which shows contour plots of the density for both runs.

The case described above suggests that the system has a supercritical mass to flux ratio (Mouschovias & Spitzer 1976), since the magnetic field is not able to stop the collapse. This behavior is still observed with  $B_o = 2.5$ , but at  $B_o = 3$  the system again does not collapse in spite of the production of fluctuations exceeding  $\rho = 55$ , suggesting that the system has become subcritical. We performed new runs with the B-model, no forcing and  $\nu_2 = \eta = 0.04$ , taking as initial conditions zero velocity dispersion and the mass concentrated in a wide Gaussian profile at the center of the box with  $\gamma_e = 0.9$ , a choice of parameter that permits to avoid violent initial collapse transients. For both  $B_o = 3$  and  $B_o = 4$  the system reaches an equilibrium. Starting now new simulations from these equilibrium states with  $\gamma_e = 0.3$  leads, for  $B_o = 4$ , to a new equilibrium with a higher density peak, while for  $B_o = 3$  the system collapses, indicating that for that value of  $B_o$ , thermal pressure is still needed to fight gravity. As a result we can argue that an arbitrary high level of turbulence would not be able to produce gravitational collapse for  $B_o = 4$ , whereas if a strong enough fluctuation could gather enough mass, collapse could occur with  $B_o = 3$ .

Thus, at a fixed value of  $J$ , there are two critical values of the uniform field  $B_o$ : one ( $B_1$ ) to provide linear stability of the slab state, and the other ( $B_2 > B_1$ ) corresponding to the transition from supercritical to subcritical. According to our results, turbulence is able to shift  $B_1$  to higher values as turbulent fluctuations lose thermal support (at small enough  $\gamma_e$ ). However, it does not seem to be able to modify  $B_2$ . We speculate that  $B_1$  should tend to  $B_2$  as thermal

support is weakened ( $\gamma_e \rightarrow 0$ ). Therefore, the mass-to-flux ratio criterion appears to be very robust to the presence of strong nonlinearities (at the large scale), as it is based solely on global conservation conditions. However, we note that the presence of small-scale MHD turbulence inside the condensations themselves, which we cannot follow here due to the limited resolution, could in principle provide, through reconnection, a dissipation of the magnetic field allowing for an increase of the mass-to-flux ratio. Finally, we remark that, although turbulence appears incapable of inducing collapse of supercritical condensations, it is a necessary agent in their formation, since the slab state is linearly stable in the absence of turbulence due to the contribution from the thermal pressure.

## 5. Behavior of a thermodynamic model of the ISM at the kpc scale

In this section we test the applicability of our conclusions on the influence of  $\gamma_e$  on cloud formation and collapse scenarii in the context of the full model used in Paper II (cf. § 2) including also rotation and shear, with values adequate for the ISM at the 1 kpc scale. We have performed two simulations (runs 102 and 113) with the fiducial values described in Table 1 of Paper II, although without star formation nor random forcing ( $\Gamma_s = 0, \mathbf{F}_c = 0$ ). These two runs differ only in the value of  $\alpha$ . We do not include forcing since in this case it should be at small scales due to stellar activity, which in turn should be the outcome of gravitational collapse.

Neither run 102 nor run 113 collapse gravitationally, at least over 50 code time units. (Recall that for this model, a code time unit corresponds to  $1.3 \times 10^7$  yr and a density unit equals  $1 \text{ cm}^{-3}$ .) Since no forcing other than the large scale shear is present in runs 102 and 113, the turbulence decays after a few turnover times and we only observe the nonlinear development of the oscillations suggested by Elmegreen (1991) and described in Paper II. As in Paper II, the clouds form preferentially in regions of zero shear (since shear rotates a perturbation contracting along the field into the perpendicular direction); other runs without magnetic field (not shown) form condensations of even lower amplitude (due to the absence of magnetic braking) and in regions of minimum shear, i.e. a shear which minimizes the epicyclic frequency. The absence of runaway collapse in these runs is interesting since, according to the linear criterion of Paper II, they

should be unstable. This confirms the speculation by Elmegreen (1991) and the observation of Paper II that the development of the instability is not exponential, but oscillatory, although in the present paper the density fluctuations have reached much larger amplitudes, and their ability to rebound is remarkable. Ultimately, the possibility that they will collapse on very large time scales cannot be ruled out, but is not necessarily relevant in the context of the ISM.

In spite of the absence of gravitational collapse, the simulations support the scenario of the previous sections: the hard case ( $\alpha = 0$ ) develops only one condensation of fluctuating amplitude, reaching  $\rho_{\max} = 20$  at  $t = 14$  in code units. Instead, the  $\alpha = 0.5$  case develops a larger number of condensations, one reaching  $\rho_{\max} = 86$  at  $t = 7.6$ , which however rebounds and does not collapse. Later, this same condensation reaches  $\rho_{\max} = 95$  at  $t = 20.6$ . The evolution of the maximum density in the integration box is shown for both runs in fig. 12. The eventual dying out of such fluctuations as seen here for late times is linked to the choice  $\Gamma_s = 0$ , as discussed in Paper I and II. These condensations move along epicycles, and exhibit a wave-like behavior since there are no turbulent compressions nor instabilities of any kind (§ 3.1; see also Adams et al., 1994; Gehman et al. 1996).

The latter observation is a consequence of the well-known fact that the presence of rotation restores a “hard” behavior, analogous to a large value of  $\gamma_e$ . However, as discussed in § 3.3.1, the relative importance of the Coriolis force compared to the magnetic and nonlinear advection terms decreases at small scales, so that this scenario suggests stability of the large scales with possible instability of the small scales. Moreover, the turbulence-induced collapse of the small scales shown in § 4 should also contribute to small-scale collapse, although in particular in runs 102 and 113 this effect cannot be seen due to the absence of fully developed turbulence and to the low resolution.

## 6. Conclusions

In the present paper, we have investigated some properties of highly compressible turbulence, which is relevant in flows with very efficient cooling processes, such as the ISM or cosmological flows after the epoch of recombination. In these cases, the flow may be subsonic with respect to the isothermal sound

speed, and yet have an effectively supersonic behavior. We first considered the purely hydrodynamical regime, addressing the type of density structures formed by turbulence. We showed that the density jump in barotropic flows in the limit of small polytropic index  $\gamma_e$  approaches  $e^{M^2}$ , where  $M$  is the Mach number ahead of the shock, rendering the flow much more compressible than high Mach number regimes with  $\gamma_e \sim 1$ . When  $\gamma_e$  is small, the density structures are long-lived and object-like, i.e. carrying the mass together with the density fluctuations while, for larger values of  $\gamma_e$ , the behavior is more wave-like, and the density field consists of short-lived patches separated by shocks.

In the presence of purely compressible forcing, vorticity is observed to decay in time, even in 3D, where the dominant effect of the vortex stretching term is actually to act as a sink of potential vorticity at the location of shocks. Thus vorticity production relies heavily on other sources, such as the Coriolis force, large-scale shear originating from differential rotation, baroclinic vorticity production in the presence of local heating, and the magnetic field. For the Galactic disk, the Coriolis force is most important at large scales, while the magnetic field is most effective at the small ones (molecular clouds). The decay of vorticity we observe in the absence of those additional agents may be at the origin of the small amounts of rotation found in observational surveys of molecular clouds and their cores (e.g., Arquilla & Goldsmith 1986; Goodman et al. 1993).

With self-gravity, we have given a simple criterion for turbulent compression through shocks to produce self-gravitating structures, based on the threshold value of  $\gamma_e$  below which the Jeans mass of a turbulent density fluctuation decreases upon the compression. In particular, if the dimensionality of the compression is between 1 and 2, then the required value of  $\gamma_e$  is between 0 and 1, consistent with estimated values in the ISM (e.g., Myers 1978). Using numerical simulations, we have verified that in the presence of strongly compressible turbulence, local turbulent fluctuations can collapse even if the medium is globally stable in the linear sense, although generally requiring long times. Flows with small  $\gamma_e$  develop collapsing structures at smaller scales than flows with larger  $\gamma_e$  but with the same effective Jeans length. Flows with self-gravity and magnetic fields exhibit an analogous behavior to the purely hydrodynamic case for supercritical mass-to-flux ratios. For subcritical situations,

large-scale turbulence is incapable of inducing small-scale collapse, although it is a necessary agent for the formation of magnetically supported clouds.

These results have implications for present-day *vs.* primordial star formation, inasmuch as  $\gamma_e$  is directly related to the medium's metallicity. For the low metallicity primordial gas, we expect that turbulence will not be sufficient to produce small-scale collapsing structures due to the large values of  $\gamma_e$ , and therefore collapse can only occur through large-scale gravitational instability, leading to the formation of globular clusters. Conversely, collapsing turbulence-induced, small-scale density fluctuations may lead to formation of open clusters under present-day metallicity conditions. This problem will be investigated in detail in a forthcoming paper (Franco et al. 1996).

Fully thermodynamic models incorporating magnetic fields, rotation and shear with parameters appropriate to the modeling of the ISM at the kpc scale (c.f. Paper II) but without stellar heating ( $\Gamma_s = 0$ ) develop highly nonlinear wave-like structures which however do not collapse gravitationally. Their behavior is analogous to the hydrodynamic case with a larger  $\gamma_e$  and initial turbulent transients are not capable of forming small-scale self-gravitating structures. Thus, in order to obtain collapse of the large scales an instability is required. On the other hand, small-scale collapse in the clouds should also occur, since rotation is less efficient at those scales and we have shown that turbulence also induces it. This is not observable in the simulations presented in this paper due to their low resolution, but may be seen at higher resolutions.

A final remark is that in this paper we have investigated the effects of large-scale turbulence on structure formation in highly compressible flows, but have neglected small-scale effects, such as those mentioned above, as well as turbulent pressure support and reconnection of small-scale magnetic fluctuations, which could possibly modify the mass-to-flux ratio and allow for an increased compressibility of the flow. The simultaneous investigation of both aspects of turbulence requires very high resolution simulations, which will be presented elsewhere.

We are glad to acknowledge John Scalo for useful comments and suggestions, and a critical reading of the manuscript. The numerical simulations were performed on the Cray C98 of IDRIS, CNRS, France, and the Cray Y-MP 4/64 of DGSCA, UNAM, México. This work has made use of NASA's Astrophysical

Data System Abstract Service. We thankfully acknowledge financial support from UNAM/CRAY grant SC-002395 to E. V.-S., and a joint CONACYT-CNRS grant.

## REFERENCES

- Adams, F. C., Fatuzzo, M., Watkins, R. 1994, ApJ, 426, 629
- Arquilla, R., & Goldsmith, P. F. 1986, ApJ, 303, 356
- Bonazzola, S., Falgarone, E., Heyvaerts, J., Pérault, M., Puget, J. L. 1987, A&A 172, 293
- Chandrasekhar, S. 1951, Proc. R. Soc. London, 210, 26
- Chandrasekhar, S. 1961, Hydrodynamic and Hydro-magnetic Stability (Oxford: Clarendon)
- Dalgarno, A., McCray, R. A. 1972, ARAA, 10, 375
- Elmegreen, B. G. 1989, ApJ, 344, 306
- Elmegreen, B. G. 1991, ApJ, 378, 139
- Elmegreen, B. G. 1993a, ApJ (Lett.), 419, L29
- Elmegreen, B. G. 1993b, in Protostars and Planets III, ed. E. H. Levy, J. I. Lunine (Tucson: Univ. of Arizona Press), 97
- Evans, N. J. 1991, in Frontiers of Stellar Evolution, ed. D. Lambert (San Francisco: A.S.P), 45
- Falgarone, E., Phillips, T. G., Walker, C. K. 1991, ApJ, 378, 186
- Falgarone, E., Puget, J.-L. & Pérault, M. 1992, A&A, 257, 715
- Fleck, R. C. 1991, Ap&SS, 182, 81
- Fleck, R. C. 1996, ApJ, 458, 739
- Franco, J. J., Vázquez-Semadeni, E., Passot, T. 1996, in preparation
- Gehman, C. S., Adams, F. C., Fatuzzo, M., Watkins, R. 1996, ApJ, 457, 718
- Goodman, A. A., Benson, P. J., Fuller, G. A., & Myers, P. C. 1993, ApJ, 406, 528
- Hayes, W. D. 1957, J. Fluid Mech., 2, 595
- Hoyle, F. 1953, ApJ, 118, 513

- Hunter, J. H. Jr., & Fleck, R. C. 1982, *ApJ*, 256, 505
- Hunter, J. H. Jr., Sandford, M. T. II, Whitaker, R. W. & Klein, R. I. 1986, *ApJ*, 305, 309
- Kadomtsev, B. B., Petviashvili, V. I. 1973, *Dokl. Akad. Nauk SSSR*, 208, 794
- Kida S., Orszag S.A., 1990a, *J. of Sci. Comp.*, 5, 85.
- Kida S., Orszag S.A., 1990b, *J. of Sci. Comp.*, 5, 1.
- Klein, R. I., McKee, C. F. 1994, in *Numerical Simulations in Astrophysics: Modeling the Dynamics of the Universe*, ed. J. Franco, S. Lizano, L. Aguilar, E. Daltabuit, (Cambridge: Univ. Press), 251
- Kornreich, P., Scalo, J. 1996, in preparation
- Krause, F., Rädler, K. H. 1980, *Mean Field MHD and Dynamo Theory* (Oxford: Pergamon)
- Larson, R. B. 1981, *MNRAS*, 194, 809
- Léorat, J., Passot, T., & Pouquet, A. 1990, *MNRAS*, 243, 293
- McKee, C. F., Zweibel, E. G. 1992, *ApJ*, 399, 55
- Mouschovias, T. C. 1991, in *The Physics of Star formation and Early Stellar Evolution*, Ed. C. J. Lada, N. D. Kylafis (Dordrecht: Kluwer) 61
- Mouschovias, T. C., Spitzer, L. Jr. 1976, *ApJ*, 210, 326
- Myers, P. C. 1978, *ApJ*, 225, 380
- Padoan, P. 1995, *MNRAS*, 277, 377
- Passot T., Vázquez-Semadeni E., Pouquet A., 1995, *ApJ*, 455, 702 (Paper II)
- Passot T., Pouquet A., 1987, *J. Fluid Mech.*, 181, 441
- Passot T., Pouquet A., Woodward P.R., 1988, *A&A*, 197, 228
- Passot T., Pouquet A., 1988, *J. Comp. Phys.* **75**, 300
- Pedlovsky, J. 1987, *Geophysical Fluid Dynamics* (2nd ed.) (New York: Springer)
- Porter, D. H., Pouquet, A., Woodward, P. R. 1994, *Phys. Fluids*, 6, 2133
- Porter, D. H., Pouquet, A., Woodward, P. R. 1995, in *Small-Scale Structures in Three-Dimensional Hydrodynamic and Magnetohydrodynamic Turbulence*, ed. M. Meneguzzi, A. Pouquet, P.-L. Sulem (Berlin: Springer), 51
- Renard, M., Chiéze, J. P. 1993, *A&A*, 267, 549
- Scalo, J. M., & Struck-Marcell, C. 1984, *ApJ*, 276, 60
- Scalo, J. M. 1987, in *Interstellar Processes*, ed. D. J. Hollenbach, H. A. Thronson (Dordrecht: Reidel), 349
- Spitzer, L., Savedoff, M. P. 1950, *ApJ*, 111, 593
- Stevens, I. R., Blondin, J. M., & Pollack, A. M. T. 1992, *ApJ*, 386, 265
- Vázquez-Semadeni E., Passot T., Pouquet A., 1995, *ApJ*, 441, 536 (Paper I)
- Vázquez-Semadeni, E., Gazol, A. 1995, *A&A*, 303, 204
- Vázquez-Semadeni E., Passot T., Pouquet A., 1995, in *Proceedings of the fifth Mexico-Texas conference on astrophysics: gaseous nebulae and star formation*, *Rev. Mex. A.A. Ser. Conf.* **3**, 61.
- Vishniac E.T., 1983, *ApJ*, 274, 152.
- Vishniac E.T., 1994, *ApJ*, 428, 186
- Vishniac E.T, Diamond P., 1992, *ApJ*, 398, 561.

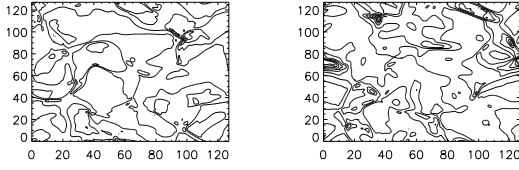


Fig. 1.— Contours of the density field for run 63 ( $\gamma_e = 1.5$ , *left*) and run 65 ( $\gamma_e = 0.3$ , *right*) at a nondimensional time of  $t = 7.6$ . In both cases there are 10 contour levels with a constant spacing  $\Delta\rho = 0.3$ . Note the “patchy” structure of the density field, with higher peaks at the intersection of shocks in (b).

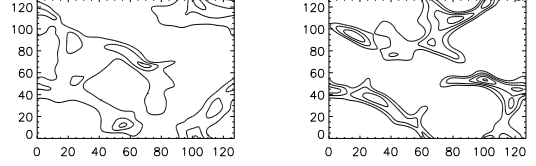


Fig. 2.— Contours of the density field of run 54 ( $\alpha = -0.5$ , *left*) and run 53 ( $\alpha = 0.5$ , *right*) at  $t = 6.0$ . The contours represent density values of  $\rho = 1, 2, 4, 8, 16, 32$ . Both runs use the *ppm* equations. Note that clouds are better defined than in fig. 1, and have higher peak densities in (b).

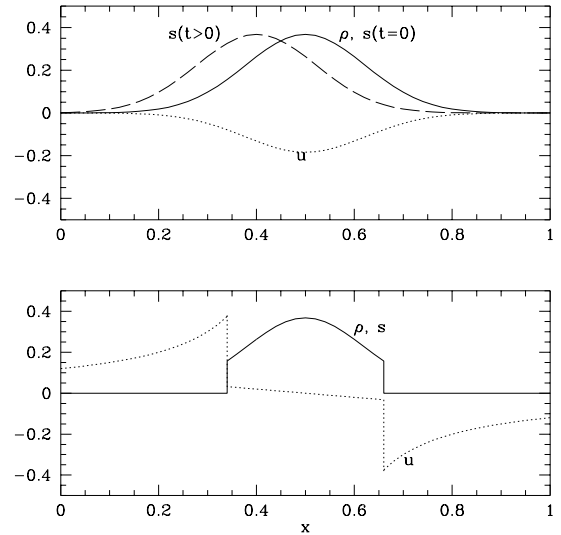


Fig. 3.— One-dimensional sketches of the density  $\rho$ , the passive scalar  $s$  and the velocity  $u$  in the case of a wave (*top*) and an object (*bottom*). In the case of the wave, the passive scalar, which represents advection of material, drifts away from the density, while in the case of the object,  $s$  remains within the density fluctuation.

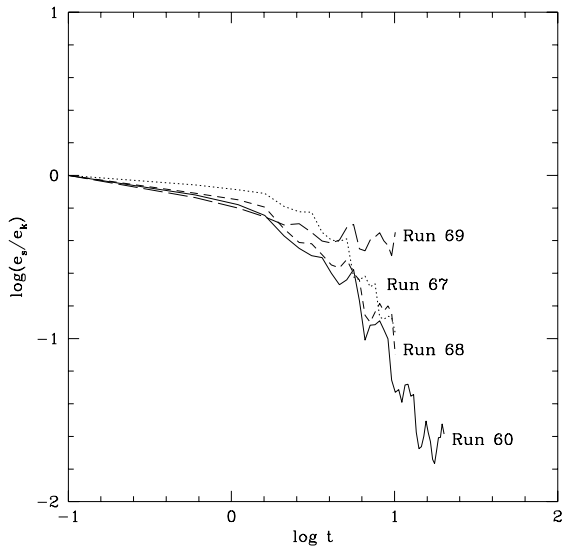


Fig. 4.— Evolution of the ratio of solenoidal to total kinetic energy per unit mass  $e_s/e_k$  for runs 60 (*solid line*), run 67 (*dotted line*), run 68 (*short-dashed line*) and run 69 (*long-dashed line*). Runs 60 and 67 are in 3D and use the *ppm* equations with  $\alpha = 0.5$  and  $\alpha = -0.5$  respectively. Run 68 is similar to run 60 but fully thermodynamic. Run 69 is similar to run 60 but includes the Coriolis force with  $\Omega = 0.4$ . After similar initial transients, the ratio  $e_s/e_k$  decays in all cases except in the run including the Coriolis force.

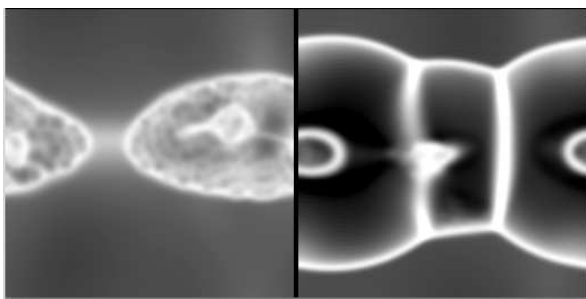


Fig. 5.— Gray-scale images of the density field for run 28 (*left*) and run 35 (*right*). Both runs are fully thermodynamic, but run 28 has local thermal forcing only, while run 35 has wind-type compressible forcing on the velocity only. The shells evolve smoothly in run 35, but distort and disrupt in run 28 due to the strong vorticity production.

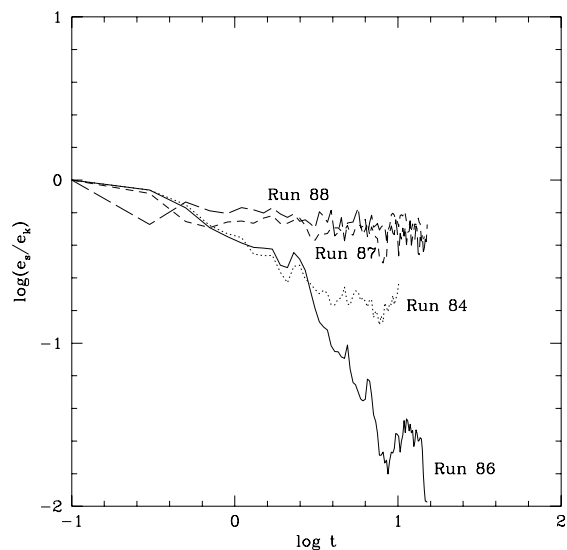


Fig. 6.— Evolution of the ratio of solenoidal to total kinetic energy per unit mass  $e_s/e_k$  for runs 86 (*solid line*), run 84 (*dotted line*), run 87 (*short-dashed line*) and run 88 (*long-dashed line*). These runs respectively have values of the initial uniform field of  $B_o = 0.05, 0.3, 1$  and  $3$ . The final value of  $e_s/e_k$  is seen to increase with  $B_o$  until saturation at the equipartition level is reached for  $B_o > 1$ .

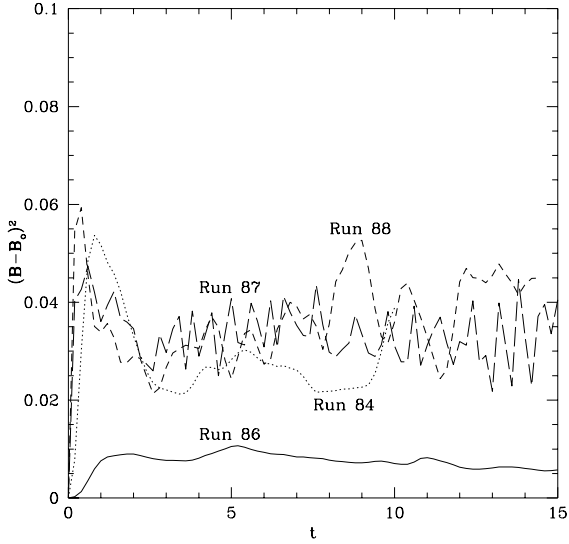


Fig. 7.— Evolution of the fluctuating magnetic energy for the same runs as in fig. 6, using the same line coding. A similar trend of increasing strength with  $B_0$  is observed, with saturation at  $B_0 > 1$ . Note also the increasing frequency of the oscillations, roughly proportional to  $B_0$ .

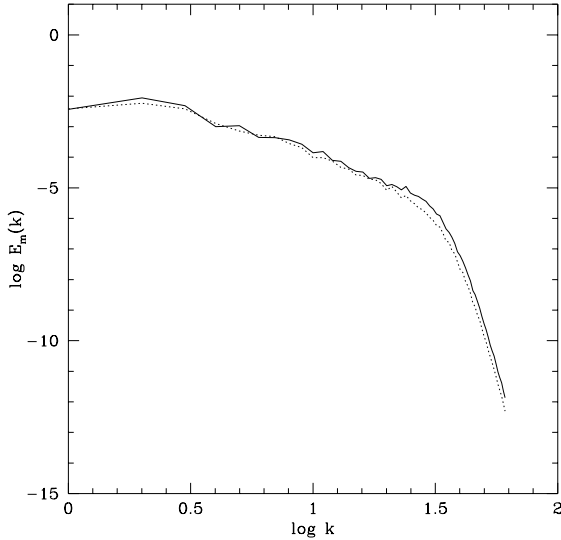


Fig. 8.— Spectra of the  $x$ - and  $y$ -components of the magnetic field of run 87 at  $t = 14.4$ . A well-defined power-law inertial range is observed, indicative of fully developed turbulence.

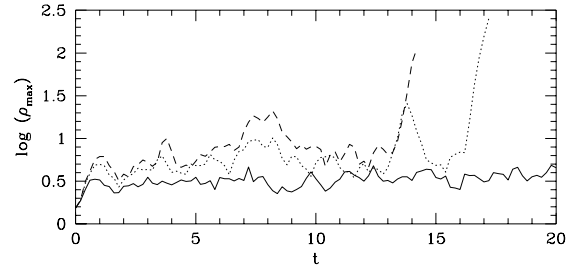


Fig. 9.— Evolution of the maximum density for runs 106 (*solid line*), 107 (*dotted line*) and 108 (*dashed line*), which respectively have  $\gamma_e = 0.9, 0.3$  and  $0.1$ , all with  $J = 0.9$ , implying linear stability. Turbulent fluctuations of finite strength are seen to be able to collapse gravitationally for runs 107 and 108 in spite of the global linear stability.

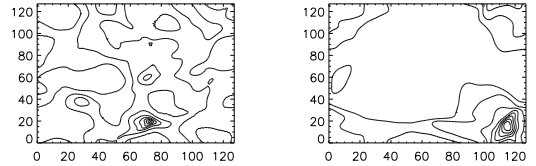


Fig. 10.— Contour plots of the density fields of runs 108 (*left*) and 109 (*right*), which respectively have  $J = 0.9$  and  $1.1$ . Run 109 is thus linearly unstable, and the collapse is seen to involve most of the mass in the simulation, while the turbulence-induced collapse in run 108 is local. The contours denote the values  $\rho = 0.5, 1, 2, 4, 8, 16, 32$  and  $64$ .

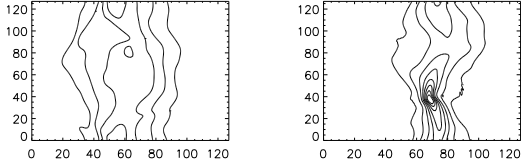


Fig. 11.— Contour plots of the density fields of runs 111 (*left*) and 114 (*right*), both permeated by a uniform magnetic field of strength  $B_o = 0.2$  in the  $x$ -direction and with  $J = 1.1$ . Run 111 has  $\gamma_e = 0.9$ , and for run 114,  $\gamma_e = 0.3$ . Being linearly unstable, both runs contract to a slab. Turbulent fluctuations, however, manage to produce a subcondensation in run 114 which finally collapses gravitationally. The contour spacing is identical to that of fig. 10.

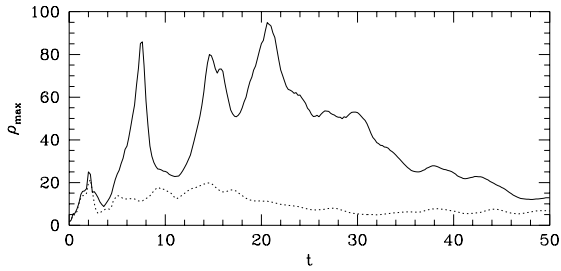


Fig. 12.— Evolution of the maximum density for runs 102 (*solid line*) and run 113 (*dotted line*). Both runs include rotation, shear and magnetic field, in the context of the full model of Paper II, but without star formation. Although not collapsing gravitationally, both runs exhibit strong density fluctuations.

**Table 1.** Run parameters

Run #	Type <sup>a</sup>	Forcing <sup>b</sup>	$(e_s/e_k)_0^c$	Shear <sup>d</sup>	$J^e$	$B_0^f$	$\Omega^g$	$\gamma_e^h$	$\alpha^i$
28	T2D	W	0	N	0	0	0.0	N/A	0.5
35	T2D	T	0	N	0	0	0.0	N/A	0.5
53	ppm2D	R	1	N	0	0	0	N/A	0.5
54	ppm2D	R	1	N	0	0	0	N/A	-0.5
57	ppm2D	R	1	N	0	0	0.4	N/A	0.5
59	ppm2D	R	1	Y	0	0	0.0	N/A	0.5
60	ppm3D	R	1	N	0	0	0	N/A	0.5
63	B2D	R	1	N	0	0	0	1.5	N/A
65	B2D	R	1	N	0	0	0	.3	N/A
67	ppm3D	R	1	N	0	0	0	N/A	-0.5
68	T3D	R	1	N	0	0	0	N/A	0.5
69	ppm3D	R	1	N	0	0	0.4	N/A	0.5
84	ppm2D	R	1	N	0	0.3	0	N/A	0.5
85	ppm2D	R	1	N	0	0	0.05	N/A	0.5
86	ppm2D	R	1	N	0	0.05	0	N/A	0.5
87	ppm2D	R	1	N	0	1.	0	N/A	0.5
88	ppm2D	R	1	N	0	3.	0	N/A	0.5
102	T2D	N/A	1	Y	.51	.3	0.4	N/A	0.5
106	B2D	R	1	N	0.9	0.0	0	0.9	N/A
107	B2D	R	1	N	0.9	0.0	0	0.3	N/A
108	B2D	R	1	N	0.9	0.0	0	0.1	N/A
109	B2D	R	1	N	1.1	0.0	0	0.9	N/A
111	B2D	R	1	N	1.1	2.0	0	0.9	N/A
113	T2D	N/A	1	Y	.51	.3	0.4	N/A	0.
114	B2D	R	1	N	1.1	2.0	0	0.3	N/A

**Table 1**

Main characteristics of the runs described in this paper, together with the run number. All runs except run 35 exclude stellar heating (i.e. with  $\Gamma_s = 0$  in (3)). Computations are done on a uniform grid of either  $128^2$  or  $64^3$  points, using a pseudo-spectral method with hyperviscosity. For more detail on the implementation of the physical terms and in the nondimensionalization of the equations, see text and Paper I and II.

<sup>a</sup> Types of computations: *T2D* (resp. *T3D*) refers to the full thermodynamical equations (1) – (9) written in §2, integrated in two space dimensions (resp. three); *ppm2D* (resp. *ppm3D*) refer to a simplification of the full equations in which a *piecewise polytropic model* (see (10)) is used in two (resp. three) dimensions; and finally *B2D* (resp. *B3D*) correspond to the further simplification of a barotropic law in two (resp. three) dimensions.

<sup>b</sup> The type of forcing used in the different models can be either: (R), a random forcing with a steep ( $\sim k^{-4}$ ) spectrum; (T), a thermal energy forcing with  $\Gamma_s \neq 0$ ; or finally (W), a wind with  $\mathbf{F}_c = -\nabla\psi$  with  $\psi \sim \Gamma_s$ .

<sup>c</sup>  $(e_s/e_k)_0$  is the ratio at  $t = 0$  of the rotational to total kinetic energy.

<sup>d</sup> Y (resp. N) indicates the presence (resp. absence) of shear in the computation.

<sup>e</sup>  $J$  is the gravitational parameter and measures the number of Jeans masses in the flow; when  $J = 0$ , no self-gravity is included.

<sup>f</sup>  $B_o$  is the mean magnetic field;  $B_o = 1$  corresponds to an Alfvén velocity equal to the rms turbulent velocity (see Paper II). In this column,  $B_o \equiv 0$  indicates a non-magnetic run.

<sup>g</sup>  $\Omega$  measures the intensity of the Coriolis force, independently of the externally imposed shear.

<sup>h</sup>  $\gamma_e$  is the effective polytropic exponent used in the purely barotropic (B) models (see text).

<sup>i</sup>  $\alpha$  is the exponent of the density used in a model of diffuse heating (see Paper II). The relationship between  $\alpha$  and  $\gamma_{ei}$ , the set of effective polytropic exponents appearing in the *ppm* models is given in eq. (11).